

PHYSICS-INFORMED LSTM-BASED LONGITUDINAL STALL AEROFYNAMIC MODELING FRAMEWORK OF CIVIL AIRCRAFT USING FLIGHT TEST DATA

Jinhan Wang[1], Lixin Wang[1], Rong Zhao[2], Zhao Wu[2], Yifei Xu[1], Hailiang Liu[1], Shang Tai[1] & Ting Yue[1]

[1] School of Aeronautic Science and Engineering, Beihang University, Beijing 100191, China
[2]COMAC Shanghai Aircraft Customer Service Co. Ltd., Shanghai 200241, China

Abstract

The accurate modeling of unsteady stall aerodynamics remains a challenging problem in civil aviation due to its strong nonlinearity and inherent time dependence. Neural-network-based methods offer promising modeling capabilities but often suffer from overfitting when applied to flight-test data, leading to physically inconsistent results. To address this issue, a physics-informed Long Short-Term Memory (PI-LSTM) framework for longitudinal stall aerodynamic modeling using flight-test data is proposed. In addition to the conventional prediction-error loss derived from the equations of motion, physical information is incorporated into the training objective. High-confidence aerodynamic characteristics identified from flight-test data are utilized as prior knowledge to construct three physics-informed loss terms: a proportionality constraint between the lift and pitching-moment increments induced by elevator deflection, a constraint on pre-stall static aerodynamic derivatives, and a constancy constraint on dynamic derivatives in the regular angle-of-attack region. These physics-informed loss function are jointly optimized with the prediction error loss function during network training. The proposed approach is validated using stall flight-test data from a civil aircraft. Results demonstrate that the proposed framework effectively mitigates overfitting in neural-network-based aerodynamic modeling while maintaining both high predictive accuracy and physical consistency.

Keywords: Longitudinal Stall Aerodynamic Modeling, Civil Aircraft, Flight-Test Data, Physics-informed Long Short-Term Memory (PI-LSTM), Flight simulation, Network.

1. Introduction

Since the introduction of new aviation regulations in 2019, simulator-based stall recovery training has become a mandatory requirement for airline pilots[1][2]. Consequently, high-fidelity aerodynamic models capable of accurately reproducing aircraft behavior at high angles of attack have become increasingly important for Upset Prevention and Recovery Training (UPRT)[3]. During stall conditions, civil aircraft exhibit pronounced nonlinear and unsteady aerodynamic characteristics, making the development of accurate mathematical models for stall aerodynamics a longstanding challenge in flight dynamics and system identification.

At present, stall aerodynamics of civil aircraft are predominantly modeled using physics-based analytical approaches, such as differential-equation models[4] and the Goman–Khrabrov model[5]. These models possess clear physical interpretability and describe unsteady stall effects using a limited number of parameters. However, when their parameters are identified from stall flight-test data, the resulting estimates often exhibit considerable uncertainty and dispersion due to limited excitation, strong parameter coupling, and measurement errors[6][7]. Such issues can significantly degrade model accuracy and generalization capability.

With the rapid development of machine-learning techniques, neural-network-based methods have attracted increasing attention in aerospace applications[8][9][10]. Among them, Long Short-Term Memory (LSTM) networks have demonstrated considerable potential for unsteady aerodynamic

modeling because of their ability to capture temporal dependencies and memory effects[11]. Previous studies have shown that LSTM- and Bi-LSTM-based approaches can accurately reproduce complex high-angle-of-attack aerodynamic behavior and post-stall maneuvering characteristics[12][13]. Compared with conventional parametric models, neural networks do not require a predefined aerodynamic model structure and offer superior capability for representing highly nonlinear aerodynamic phenomena. Nevertheless, most existing studies have relied on dynamic wind-tunnel data, whereas intelligent stall aerodynamic modeling directly based on flight-test data has received comparatively little attention.

Although wind-tunnel testing provides valuable aerodynamic information, scale effects and Reynolds-number discrepancies prevent it from fully reproducing the high-angle-of-attack characteristics of full-scale civil aircraft[14]. Consequently, flight-test data remain the most reliable source for obtaining realistic stall aerodynamic behavior. However, stall flight-test data are typically characterized by significant measurement noise, large uncertainties, and strong multicollinearity among flight-state variables. Under such conditions, neural-network-based models are prone to overfitting, resulting in models that may achieve excellent agreement with training data while violating fundamental aerodynamic principles. Therefore, existing LSTM-based aerodynamic modeling methods cannot be directly transferred to stall flight-test applications.

It is worth noting that, despite the complexity of the unsteady aerodynamics during stall, certain aerodynamic characteristics can still be identified from flight-test data with relatively high confidence. Examples include the pre-stall lift-curve slope, elevator control derivatives, and dynamic derivatives in the low-angle-of-attack region. These quantities represent physically meaningful aerodynamic properties of the aircraft and can therefore serve as valuable prior knowledge for model development. Incorporating such information into the training process has the potential to improve both the physical consistency and generalization capability of neural-network-based aerodynamic models.

To address these challenges, this paper proposes a Physics-Informed Long Short-Term Memory (PI-LSTM) framework for longitudinal stall aerodynamic modeling using flight-test data. High-confidence aerodynamic derivatives identified from flight-test data are incorporated as prior physical knowledge. The discrepancies between these identified derivatives and the corresponding derivatives predicted by the excited LSTM network are formulated as physics-informed loss terms and integrated into the overall training objective. By combining the nonlinear modeling capability of LSTM networks with physically meaningful aerodynamic constraints, the proposed framework enables the development of an interpretable and physically consistent stall aerodynamic model. Finally, the effectiveness of the proposed approach is demonstrated using stall flight-test data from a representative civil transport aircraft.

2. Stall Aerodynamic Modeling Framework Based on PI-LSTM

During civil-aircraft stall maneuvers, aerodynamic forces depend not only on the instantaneous flight state but also on its time history. Therefore, an LSTM network is adopted to model the aerodynamic behavior. To achieve accurate prediction of aerodynamic characteristics from stall flight-test data while ensuring physical consistency and model interpretability, a Physics-Informed Long Short-Term Memory (PI-LSTM) framework for longitudinal stall aerodynamic modeling is proposed, as illustrated in Figure 1. The main workflow is summarized as follows:

A sequence of flight-state variables is fed into the LSTM network to predict the longitudinal aerodynamic coefficients. The mean squared error between the predicted coefficients and those calculated from flight-test data is used to construct the prediction-error loss.

- Aerodynamic parameter identification is performed using the Goman–Khrabrov state-space model and flight-test data. The identified aerodynamic characteristics exhibiting low dispersion are selected as prior physical information.
- Specific state-variable sequences are used to excite the LSTM network, from which characteristic aerodynamic derivatives are extracted. The deviations between these derivatives and the corresponding prior physical information are formulated as physics-informed loss function terms.
- The prediction-error loss and physics-informed losses are combined through weighted summation to form the overall loss function. The network parameters are then iteratively updated

until convergence is achieved.

- After convergence, the trained PI-LSTM aerodynamic model is employed for subsequent flight-dynamics simulation and analysis.

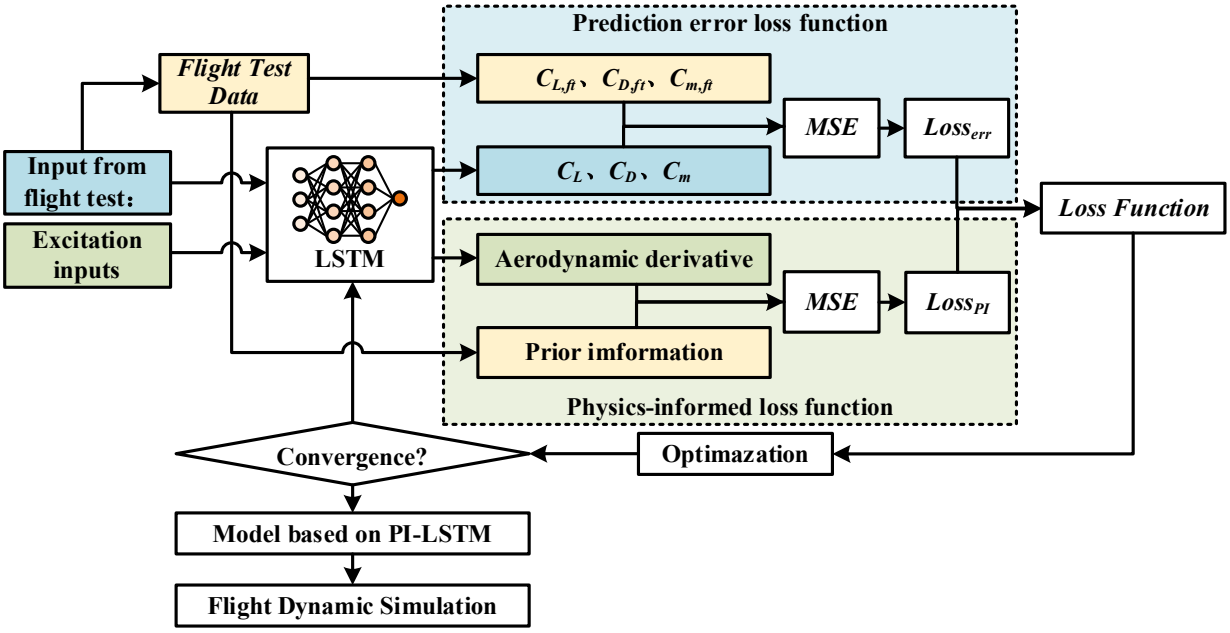


Figure 1 Stall aerodynamic modeling framework using flight-test data based on PI-LSTM

2.1 Aerodynamic Model structure Based on PI-LSTM

During stall flight tests, the longitudinal aerodynamics of a civil aircraft are governed by static aerodynamic effects, elevator-induced effects, quasi-steady dynamic effects associated with pitch rate and angle-of-attack rate, and unsteady effects arising from flow separation. Accordingly, the angle of attack (α), angle-of-attack rate ($\dot{\alpha}$), pitch rate (q), and elevator deflection (δ_e) are selected as the input state variables.

Since stall aerodynamics exhibit pronounced memory effects, the aerodynamic forces and moments depend not only on the instantaneous flight state but also on its temporal evolution. To capture such unsteady characteristics, a sequence of 50 consecutive state samples is used as the network input, denoted by X . The network output, denoted by Y , consists of the predicted lift, drag, and pitching-moment coefficients, while the observation vector Z is constructed from the corresponding aerodynamic coefficients calculated from flight-test data.

The resulting input–output relationship of the PI-LSTM aerodynamic model can be expressed as follows:

$$\begin{aligned} S &= [\alpha \quad \dot{\alpha} \quad q \quad \delta_e]^T \\ X &= [S(t-n) \quad S(t-n+1) \quad \ldots \quad S(t)] \\ Y &= [C_L(t+1) \quad C_D(t+1) \quad C_m(t+1)]^T \\ Z &= [C_{L,ft} \quad C_{D,ft} \quad C_{m,ft}]^T \end{aligned} \tag{1}$$

where n represents the length of the input time series and t denotes the discrete time index. The observation vector Z can be calculated from the flight-test data using Eq.(2):

$$\begin{cases} C_L = -C_Z \cos\alpha + C_X \sin\alpha \\ C_D = -C_X \cos\alpha - C_Z \sin\alpha \\ C_m = I_y \dot{q} / (QSc) \end{cases} \tag{2}$$

The axial-force coefficient C_X and normal-force coefficient C_Z can be expressed as:

$$\begin{cases} C_X = (mgn_x - T) / (QS) \\ C_Z = mgn_z / (QS) \end{cases} \tag{3}$$

where Q denotes the dynamic pressure, S denotes the aircraft reference wing area, and n_x and n_z

denote the axial and normal load factors, respectively.

2.2 Prediction Error Loss

Based on flight-test data, the aerodynamic forces and moment coefficients at each time instant can be inferred from measurements such as load factor and angular accelerations. Accordingly, the prediction error loss can be defined as:

$$Loss_{err} = \sum_{i=1}^{n} (Z_t - Y_t)^2 \tag{4}$$

where i denotes the discrete time index, Z represents the aerodynamic coefficients inferred from flight-test data.

2.3 Physics-informed Loss

To prevent the neural network from overfitting and to improve its interpretability, physics-informed constraints are introduced during training, which include three main aspects:

- The increments of lift and pitch moment caused by elevator are proportional.
- During the pre-stall quasi-steady phase, the lift-curve slope and elevator derivatives can be accurately identified, which should be closely matched by the LSTM outputs.
- The dynamic derivatives at low AoA are expected to remain constant.

To facilitate the extraction of individual aerodynamic components and aerodynamic derivatives, the aerodynamic coefficients predicted by the LSTM network are decomposed as follows:

$$\begin{aligned} Y(1) &= C_L[S(t-n) \quad S(t-n+1) \quad ... \quad S(t)] \\ Y(2) &= C_D[S(t-n) \quad S(t-n+1) \quad ... \quad S(t)] \\ Y(3) &= C_m[S(t-n) \quad S(t-n+1) \quad ... \quad S(t)] \end{aligned} \tag{5}$$

(1) The Increments of Lift and Pitch Moment Caused by Elevator are Proportional

The pitching moment due to elevator deflection $\Delta C_{m\delta e}$, can be regarded as the lift increment caused by the elevator deflection $\Delta C_{L\delta e}$ acting at a certain distance behind the aircraft center of gravity. Consequently, the two quantities satisfy the following relationship:

$$\Delta C_{m\delta e} = (-\frac{l_e}{c}) \Delta C_{L\delta e} \tag{6}$$

where l_e denotes the distance between the aerodynamic center of the elevator-induced lift and the aircraft center of gravity, and c is the mean aerodynamic chord of the aircraft. For a given angle of attack, the state vector is specified as:

$$\begin{aligned} S_{\alpha i}(t-n) = S_{\alpha i}(t-n+1) = S_{\alpha i}(t) &= [\alpha i \quad 0 \quad 0 \quad 0]^T \\ S_{\alpha ie}(t-n) = S_{\alpha ie}(t-n+1) = S_{\alpha ie}(t) &= [\alpha i \quad 0 \quad 0 \quad \delta_e]^T \end{aligned} \tag{7}$$

where α_i denotes the sampled AoAs over the entire range, with a sampling interval of 0.1°adopted in this study. The aerodynamic coefficients corresponding to the two input sequences are evaluated by the LSTM network. The difference between the two outputs represents the aerodynamic increment induced by elevator deflection, which can be expressed as：

$$\begin{aligned} \Delta C_L(\alpha i, \delta_e) &= C_L[S_{\alpha ie}(t-n) \quad S_{\alpha ie}(t-n+1) \quad ... \quad S_{\alpha ie}(t)] - C_L[S_{\alpha i}(t-n) \quad S_{\alpha i}(t-n+1) \quad ... \quad S_{\alpha i}(t)] \\ \Delta C_m(\alpha i, \delta_e) &= C_m[S_{\alpha ie}(t-n) \quad S_{\alpha ie}(t-n+1) \quad ... \quad S_{\alpha ie}(t)] - C_m[S_{\alpha i}(t-n) \quad S_{\alpha i}(t-n+1) \quad ... \quad S_{\alpha i}(t)] \end{aligned} \tag{8}$$

Accordingly, the corresponding physics-informed loss term can be formulated as：

$$Loss_{PI1} = \frac{1}{n} \sum_{i=1}^{n} [\Delta C_{m\delta e}(\alpha_i, \delta_e) + \frac{l_e}{c} \Delta C_{L\delta e}(\alpha_i, \delta_e)]^2 \tag{9}$$

(2) Constraint on Static Aerodynamic Coefficient Slopes at Low AoA

Since the pre-stall phase of a stall flight test is approximately quasi-steady, the associated flight-state measurements are relatively accurate. Consequently, the static lift-curve slope and elevator control derivatives can be identified with high confidence and are selected as prior physical

information, denoted by $C_{L\alpha 0}, C_{L\delta e0}$

The lift-curve slope corresponding to the LSTM-predicted aerodynamic model can be obtained as：

$$C_{L\alpha}(\alpha)=\frac{C_L[S_{\alpha i+1}(t-n)\quad S_{\alpha i+1}(t-n+1)\quad \ldots\quad S_{\alpha i+1}(t)]-C_L[S_{\alpha i}(t-n)\quad S_{\alpha i}(t-n+1)\quad \ldots\quad S_{\alpha i}(t)]}{(\alpha_i-\alpha)} \tag{10}$$

where the input state vector $S_{\alpha i}=[\alpha_i \quad 0 \quad 0 \quad 0]^T$ ， $\alpha_i=\alpha_0+\Delta\alpha\cdot i$ 。The elevator control derivative of the LSTM-based aerodynamic model can be evaluated as:

$$C_{L\delta e}(\alpha_i)=\Delta C_L(\alpha_i,\Delta\delta_e)/\Delta\delta_e \tag{11}$$

where $\Delta C_L(\alpha,\delta_e)$ is computed according to Eq. (8), and the perturbation step is set to $1°$based on the flight-test data. It is worth noting that the lift increment and pitching-moment increment induced by elevator deflection are constrained to be proportional; therefore, constructing the loss function using either $C_{L\delta e}$ or $C_{m\delta e}$ is equivalent. In this study, only the loss function associated with $C_{L\delta e}$ is considered. Accordingly, this physics-informed loss function term is formulated as follows:

$$\begin{aligned} Loss_{PI2}&=\frac{1}{m}\sum_{i=1}^{m}[C_{L\alpha}(\alpha_i)-C_{L\alpha 0}]^2 \\ Loss_{PI3}&=\frac{1}{m}\sum_{i=1}^{m}[C_{L\delta e}(\alpha_i)-C_{L\delta e0}]^2 \end{aligned} \tag{12}$$

where the maximum value of α_i is denoted as α_m, which is smaller than the critical stall angle of attack.

(3) Constant Dynamic Derivative Constraint in Low AoA

The dynamic derivatives at low AoA, computed from the LSTM network, can be constrained to be constant at low AoA. For each AoA, a state sequence with fixed pitch rate q and AoA rate $\dot{\alpha}$ is fed into the LSTM network, from which the dynamic derivatives $C_{m\dot{\alpha}}(\alpha_i)$ and $C_{mq}(\alpha_i)$ are obtained by differentiating the output with respect to $\dot{\alpha}$ and q .

Under each fixed angle of attack, the state vector is defined as:

$$\begin{aligned} S_{\alpha\dot{\alpha}}(t-n)=S_{\alpha\dot{\alpha}}(t-n+1)=S_{\alpha\dot{\alpha}}(t)&=[\alpha \quad \dot{\alpha} \quad 0 \quad 0]^T \\ S_{\alpha\dot{\alpha}}(t-n)=S_{\alpha\dot{\alpha}}(t-n+1)=S_{\alpha\dot{\alpha}}(t)&=[\alpha \quad 0 \quad q \quad 0]^T \end{aligned} \tag{13}$$

The dynamic derivatives can be further obtained as:

$$\begin{aligned} C_{m\dot{\alpha}}(\alpha)&=\frac{C_L[S_{\alpha i\dot{\alpha}}(t-n)\quad S_{\alpha i\dot{\alpha}}(t-n+1)\quad \ldots\quad S_{\alpha i\dot{\alpha}}(t)]-C_L[S_{\alpha i}(t-n)\quad S_{\alpha i}(t-n+1)\quad \ldots\quad S_{\alpha i}(t)]}{\dot{\alpha}} \\ C_{mq}(\alpha)&=\frac{C_m[S_{\alpha iq}(t-n)\quad S_{\alpha iq}(t-n+1)\quad \ldots\quad S_{\alpha iq}(t)]-C_m[S_{\alpha i}(t-n)\quad S_{\alpha i}(t-n+1)\quad \ldots\quad S_{\alpha i}(t)]}{q} \end{aligned} \tag{14}$$

Accordingly, a loss function is defined as:

$$\begin{aligned} Loss_{PI4}&=\frac{1}{m}\sum_{i=1}^{m}[C_{m\dot{\alpha}}(\alpha_i)-\bar{C}_{m\dot{\alpha}}]^2 \\ Loss_{PI4}&=\frac{1}{m}\sum_{i=1}^{m}[C_{mq}(\alpha_i)-\bar{C}_{mq}]^2 \end{aligned} \tag{15}$$

where $\bar{C}_{m\dot{\alpha}}$ and $\bar{C}_{mq}$ denote the average values of $C_{m\dot{\alpha}}$ and C_{mq}, respectively, computed over all AoAs smaller than critical stall AoA.

In summary, the total loss function can be expressed as:

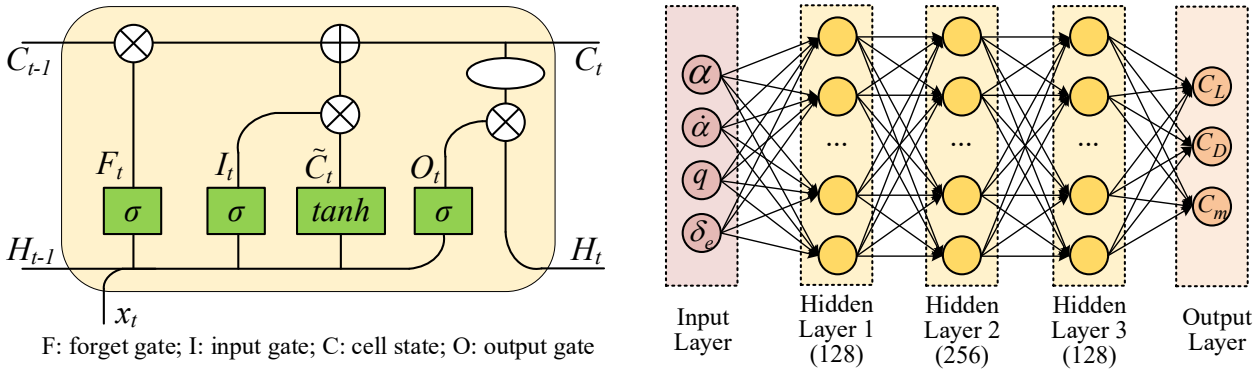
$$\begin{aligned} Loss&=Loss_{err}+wLoss_{PI} \\ &=Loss_{err}+w_1Loss_{PI1}+w_2Loss_{PI2}+w_3Loss_{PI3}+w_4Loss_{PI4}+w_5Loss_{PI5} \end{aligned} \tag{16}$$

where w_1-w_5 are the weight factors of the three components of the physics-informed loss function.

2.4 Design of the LSTM Network Structure

Long Short-Term Memory (LSTM) network is a kind of recurrent neural networks (RNNs) designed

to address long-term dependency problems by preserving information over extended time horizons. The LSTM cell architecture adopted in this study is illustrated in Figure 2(a), where the forget gate, input gate, and output gate collaboratively regulate information flow, enabling the network to capture long-range temporal dependencies in the data. The overall LSTM network architecture proposed in this work is shown in Fig. 2(b). The network consists of three layers, with 128, 256, and 128 neurons, respectively. The learning rate is set to 0.001, the batch size is 128, and the maximum number of training epochs is 100. The Adam optimizer is employed for gradient-based parameter updating.



(a) The neural unit of the LSTM **(b) The structure of the LSTM network**

Figure 2 LSTM Network Structure

Following aerodynamic modeling based on the PI-LSTM network, the fitting performance of the identified results is assessed using the goodness-of-fit (GOF) metric given in Eq.(17).

$$\mathrm{GOF} = 1 - \frac{(\boldsymbol{Z}-\boldsymbol{Y})^T(\boldsymbol{Z}-\boldsymbol{Y})}{(\boldsymbol{Z}-\boldsymbol{Z_0})^T(\boldsymbol{Z}-\boldsymbol{Z_0})} \tag{17}$$

where Z denotes the observation vector of the rolling-moment coefficient, and Z_0 represents its initial value. Y is the aerodynamic coefficient predicted by the PI-LSTM model. It is evident that $GOF \leq 1$ and a value of GOF closer to 1 indicates a better fitting performance[15].

3. Validation using actual flight-test data

The proposed stall aerodynamic modeling framework was validated using 10 stall flight-test data of a civil aircraft in takeoff configuration (flaps 15°, wingspan 27 m, weight 40 t, high-aspect-ratio design). To validate the proposed rolling-moment identification and modeling methodology, quasi-steady stall flight-test data of a civil aircraft in takeoff configuration (flap deflection of 15°) are employed for longitudinal stall modeling. The aircraft has a wingspan of approximately 27 m and a takeoff weight of about 40 t, featuring a conventional configuration with a high-aspect-ratio, low-mounted wing. As shown in Figure 3, the loss functions converge satisfactorily.

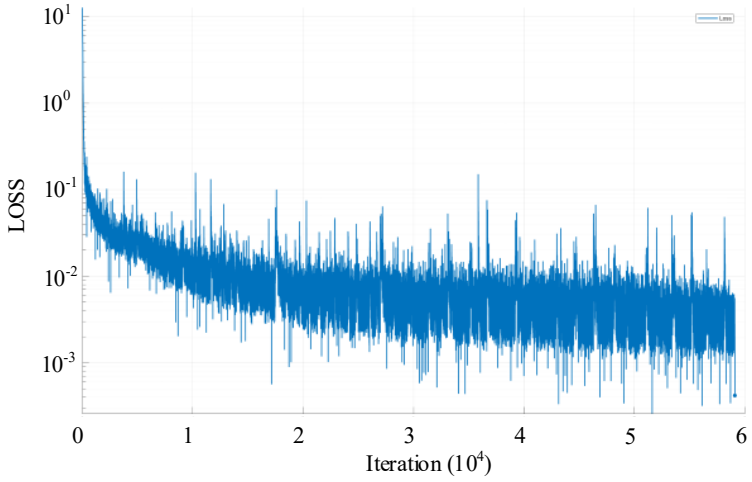


Figure 3 Loss Function Evolution During the Training Process

3.1 Fitting performance of the aerodynamic coefficients

As shown in Figure 4, the lift, drag, and pitching-moment coefficients predicted by the PI-LSTM model are compared with those reconstructed from flight-test data. The black scatter points represent the flight-test data, while the red curves denote the model predictions. Subplots (a)–(c) and (d)–(f) correspond to two different datasets, showing the lift, drag, and pitching-moment coefficients, respectively. It should be emphasized that this dataset was not used during the training process.

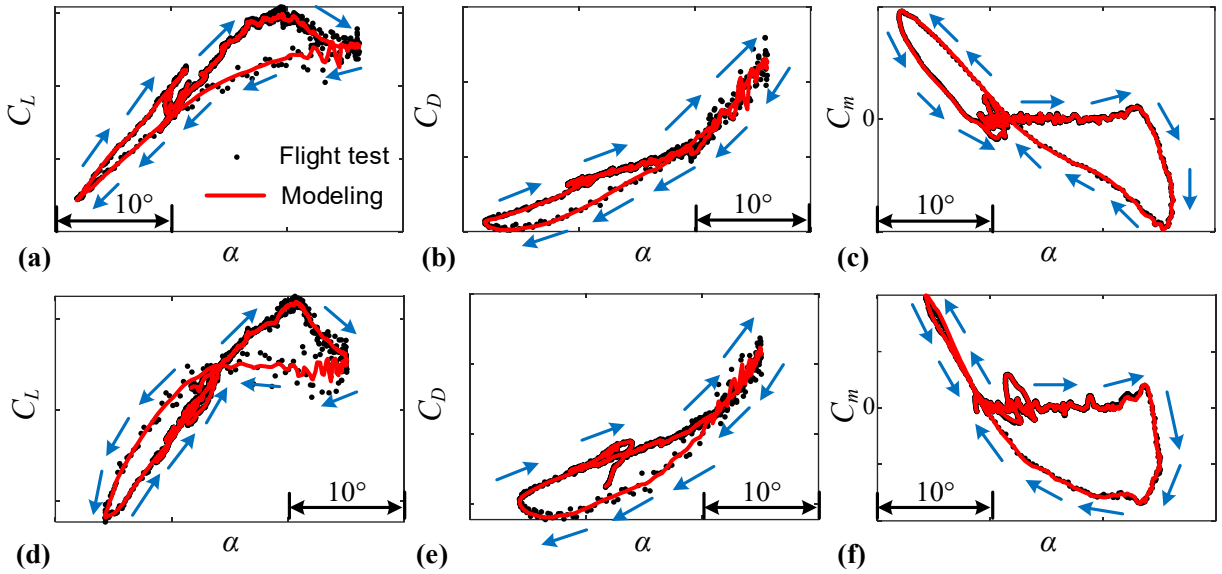


Figure 4 Fitting performance of aerodynamic coefficients

During civil-aircraft stall flight tests, a quasi-steady pre-stall regime is typically followed by a rapid recovery maneuver. As a result, the angle-of-attack rates differ significantly between the pre-stall and recovery phases. Consequently, even at the same angle of attack, the lift and drag coefficients exhibit noticeable discrepancies, reflecting pronounced unsteady aerodynamic effects throughout the maneuver. The goodness-of-fit (GOF), computed using Eq. (17), reaches 0.96 and 0.97, respectively. As illustrated in the figure, the proposed model shows good agreement with the flight-test data, indicating that the PI-LSTM-based stall aerodynamic modeling framework is capable of accurately reproducing the unsteady aerodynamic characteristics over the entire flight envelope while incorporating physical constraints. This further demonstrates that the proposed approach effectively captures the unsteady behavior of stall aerodynamics.

According to Section 2.3, representative stall aerodynamic characteristics predicted by the network are presented in Figure 5. Curves with different colors correspond to lift and pitching-moment coefficients under various elevator deflection angles. Figures 5(a) and 5(b) show the results obtained using a conventional LSTM model trained solely with prediction-error loss, without incorporating physical information. In contrast, Figures 5(c) and 5(d) present the results obtained using the proposed PI-LSTM framework, in which physics-informed loss terms are included in the training objective.

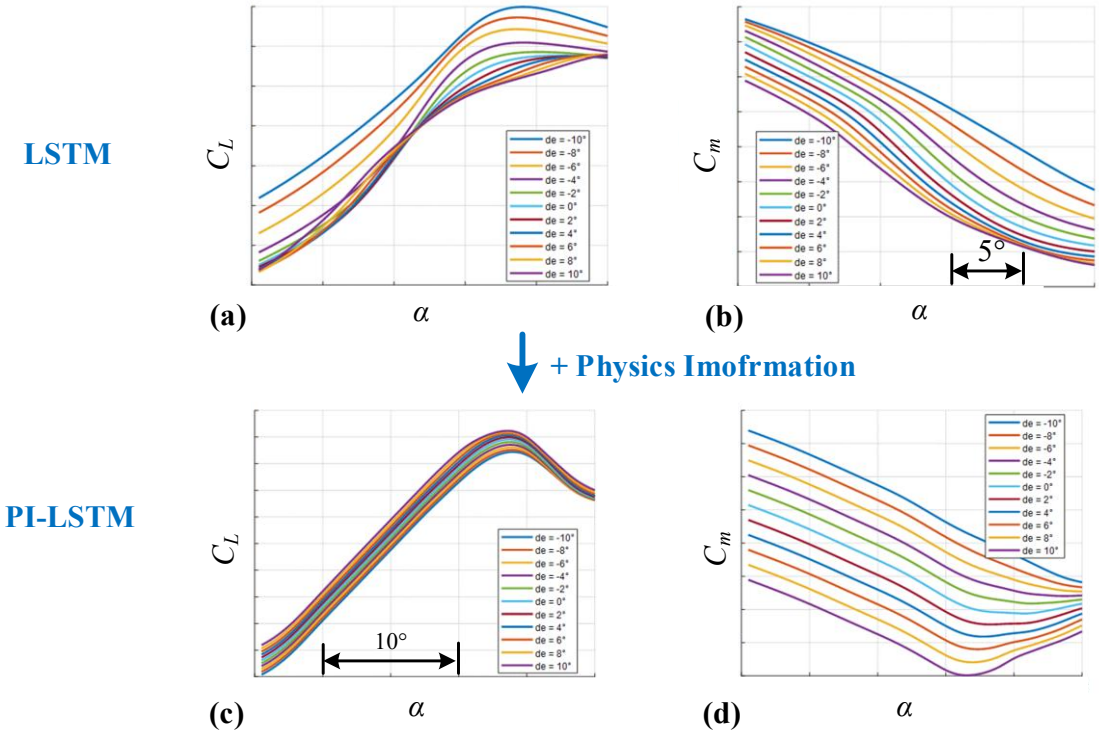


Figure 5 Static lift and pitch moment from LSTM- and PI-LSTM-based aerodynamic models

For the aerodynamic model based on conventional LSTM, the static lift and pitch moment coefficients exhibit nonlinear behavior at low AoA, and the elevator-induced increments lack clear trends, which contradicts aerodynamic principles and indicates overfit. In contrast, the aerodynamic model based on PI-LSTM yields physically consistent static aerodynamic, demonstrating that the purposed framework can effectively prevent overfitting in neural-network-based aerodynamic modeling.

3.2 Flight-dynamics simulation validation

The trained PI-LSTM aerodynamic model is coupled with the six-degree-of-freedom equations to conduct a flight dynamic simulation. Elevator deflections from the flight-test data are applied as inputs, and the flight state responses are compared with the flight test data in Figure 6. The curves represent the time histories of state variables from simulation and flight-test data, respectively. The black curves denote the tolerance bounds for high-angle-of-attack flight simulation specified in FAA 14 CFR Part 60[16].

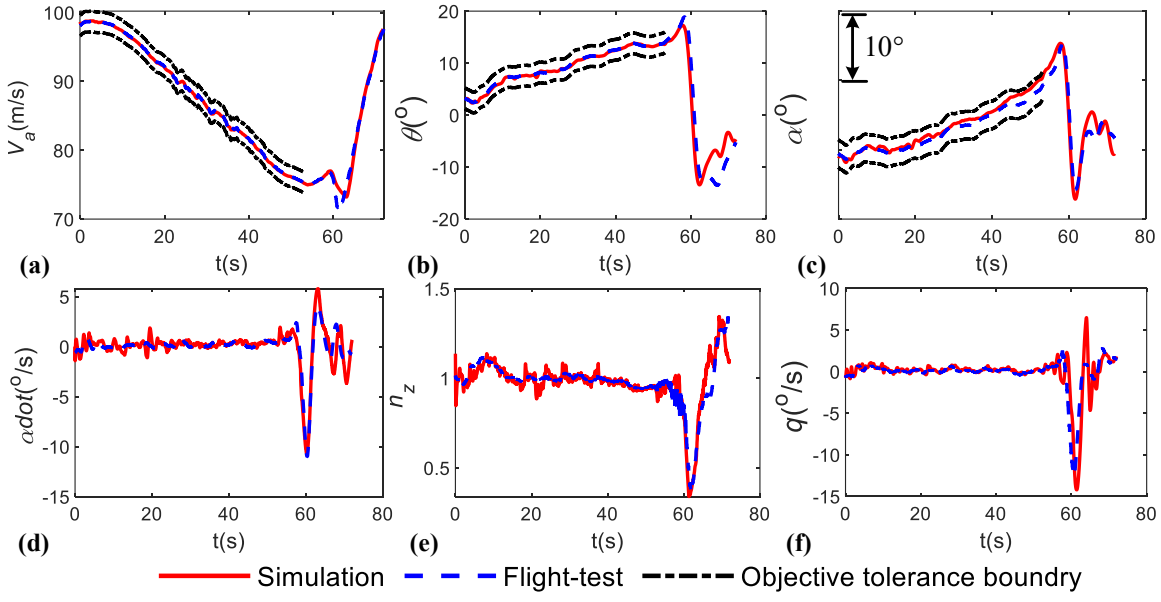


Figure 6 The comparison of response of flight dynamic model and flight test data.

It can be observed that the flight-test dataset covers an angle-of-attack range exceeding 25°, and the maximum angle-of-attack rate during the stall recovery maneuver exceeds 12°/s, adequately capturing the unsteady aerodynamic characteristics associated with both stall and recovery phases. For this dataset, under identical elevator inputs, the simulated time histories of all state variables show good agreement with the flight-test results, and the simulation results closely match the flight test data and remain within the tolerance bounds specified by FAA 14 CFR Part 60. These results demonstrate that the proposed PI-LSTM-based stall aerodynamic modeling approach is valid and effective. The resulting model not only accurately reproduces aerodynamic coefficients during stall flight, but also provides reliable predictions of state-variable time histories within a flight-dynamics simulation framework.

4. Conclusion

This paper presents a physics-informed Long Short-Term Memory (PI-LSTM) framework for longitudinal stall aerodynamic modeling of civil aircraft using flight-test data. The proposed method addresses the limitations of conventional physics-based models and data-driven neural networks in representing strongly nonlinear and unsteady stall aerodynamics under flight-test conditions.

To improve model robustness and physical consistency, high-confidence aerodynamic characteristics identified from flight-test data are incorporated as prior information. These include static lift-curve slope, elevator control derivatives, and low-angle-of-attack dynamic derivatives. Physics-informed constraints are formulated by comparing these characteristic quantities with the corresponding outputs of the LSTM network and are embedded into the overall loss function together with the standard prediction-error term.

Validation results based on stall flight-test data of a representative civil transport aircraft demonstrate that the proposed PI-LSTM model achieves high predictive accuracy. The proposed PI-LSTM model accurately reproduces the unsteady aerodynamic behavior during stall entry and recovery, particularly under large variations in angle-of-attack rate. Compared with conventional data-driven approaches, the proposed method effectively mitigates overfitting while preserving physically meaningful aerodynamic behavior.

Further flight-dynamics simulation results show good agreement between predicted and measured state-variable time histories, and all responses remain within regulatory tolerance bounds specified by FAA 14 CFR Part 60. These results confirm that the proposed framework provides a reliable and practical approach for high-fidelity stall aerodynamic modeling and flight simulation of civil aircraft.

5. Contact Author Email Address

Submitted author: Jinhan Wang: by2105407@buaa.edu.cn

Corresponding author: Shang Tai: taishang@buaa.edu.cn, Ting Yue: yueting_buaa@163.com

6. Copyright Statement

The authors confirm that they, and/or their company or organization, hold copyright on all of the original material included in this paper. The authors also confirm that they have obtained permission, from the copyright holder of any third party material included in this paper, to publish it as part of their paper. The authors confirm that they give permission, or have obtained permission from the copyright holder of this paper, for the publication and distribution of this paper as part of the ICAS proceedings or as individual off-prints from the proceedings.

References

[1] Lambregts, A., Nesemeier, G., Newman, R., & Wilborn, J. (2008, August). Airplane upsets: Old problem, new issues. In AIAA modeling and simulation technologies conference and exhibit (p. 6867).

[2] Advani, S. K., Schroeder, J. A., & Burks, B. (2016). Global implementation of upset prevention & recovery training. In AIAA Modeling and Simulation Technologies Conference (p. 1430).

[3] Foster, J., Cunningham, K., Fremaux, C., Shah, G., Stewart, E., Rivers, R., ... & Gato, W. (2005, August). Dynamics modeling and simulation of large transport airplanes in upset conditions. In AIAA Guidance, Navigation, and Control Conference and Exhibit (p. 5933).

[4] Abramov, N., Goman, M., Demenkov, M., & Khrabrov, A. (2005, August). Lateral-directional aircraft dynamics at high incidence flight with account of unsteady aerodynamic effects. In AIAA Atmospheric Flight Mechanics Conference and Exhibit (p. 6331).

[5] Goman, M., & Khrabrov, A. (1994). State-space representation of aerodynamic characteristics of an aircraft at high angles of attack. Journal of Aircraft, 31(5), 1109-1115.

[6] Delfosse, A., de Visser, C. C., & Pool, D. M. (2022). Asymmetric Stall Modeling of the Cessna Citation II Aircraft. In 6th CEAS Conference on Guidance, Navigation and Control.

[7] Wang，L., Zhao, R., & Zhang, Y. (2022). Aircraft lateral-directional aerodynamic parameter identification and solution method using segmented adaptation of identification model and flight test data. Aerospace, 9(8), 433.

[8] Wang, J., Tang, H., Liu, H., Wang, L., Chen, D., & Lu, Y. (2022, August). Design of longitudinal automatic carrier landing system based on reinforcement learning. In *International Conference on Guidance, Navigation and Control* (pp. 2964-2976). Singapore: Springer Nature Singapore.

[9] Sharma, G., & Tanimoto, J. (2024). Application of convolutional neural networks in determining the velocity and pressure fields around airfoil models. In *ICAS Proceedings*. International Council of the Aeronautical Sciences.

[10]Yue, T., Wang, X., Wang, B., Tai, S., Liu, H., Wang, L., & Jiang, F. (2025). Design of Ice Tolerance Flight Envelope Protection Control System for UAV Based on LSTM Neural Network for Detecting Icing Severity. *Drones*, *9*(1), 63.

[11]Hochreiter, Sepp, and Jürgen Schmidhuber. "Long short-term memory." *Neural computation* 9, no. 8 (1997): 1735-1780.

[12]Xiang, C. H. E. N., Jingxia, Z. H. A. N., Ke, C. H. E. N., Zhongcheng, W. E. I., & Yuan, C. A. O. (2022). Unsteady aerodynamic modeling research and virtual flight test verification. *Journal of Experiments in Fluid Mechanics*, *36*(3), 65-72.

[13]Liu, B., Shen, Y., Feng, S., Bu, C., & Tan, H. (2024, October). Research on unsteady aerodynamic modeling method based on deep neural network. In *2024 IEEE International Conference on Unmanned Systems (ICUS)* (pp. 2000-2006). IEEE.

[14]de Visser, C. C., & Pool, D. M. (2023). Stalls and Splines: Current Trends in Flight Testing and Aerodynamic Model Identification. Journal of Aircraft, 60(5), 1480-1502.

[15]Simmons, B. M., McClelland, H. G., and Woolsey, C. A. "Nonlinear model identification methodology for small, fixed-wing, unmanned aircraft," Journal of Aircraft Vol. 56, No. 3, 2019, pp. 1056-1067.

[16]FAA. "14 CFR Part 60 - Flight Simulation Training Device Initial and Continuing Qualification and Use," 2016.